Mitigating catalyst deactivation in selective hydrogenation by enhancing dispersion and utilizing reaction heat effect

Yanan Liu[1,2], Shaoxia Weng[1], Alan J. McCue[3], Baoai Fu[1], He Yu[1], Yufei He[1,2], Junting Feng[1,2], Dianqing Li[1,2,*] and Xue Duan[1]

[1]*State Key Laboratory of Chemical Resource Engineering, Beijing University of Chemical Technology, Beijing, 100029, China*

[2]*Beijing Engineering Center for Hierarchical Catalysts, Beijing University of Chemical Technology, Beijing, 100029, China*

[3]*Department of Chemistry, University of Aberdeen, Aberdeen AB24 3UE, U.K.*

* Corresponding authors

Address: *Box 98, 15 Bei San Huan East Road, Beijing, China, 100029*

Fax: *+86 (10) 6442 5385* Tel.: *+86 (10) 6445 1007*

E-mail address: *lidq@mail.buct.edu.cn (Dianqing Li)*

Abstract

Pd catalysts with different particle size were investigated in a strongly exothermic acetylene hydrogenation by changing space velocity. It was found that larger Pd nanoparticles provoked the significant amounts of oligomers and accumulated reaction heat although space velocity had been greatly improved. When Pd particle size was reduced, the number of active sites increased, which contributed to a decrease in heat produced on a single active site, thereby hindered formation of hot spots over catalyst leading to lesser deactivation. Furthermore, by utilizing the features of highly dispersed catalyst without instantaneous heat accumulation, the target acetylene hydrogenation (exothermic) was coupled with acetylene dissociation (endothermic) by sharing reaction heat to construct supported Pd carbide catalysts. Modification of subsurface carbon inhibited the generation of green oil and thus further enhanced selectivity and stability. This work provides an alternative and counter-intuitive concept where more highly dispersed metal nanoparticles may in fact be more stable.

Keywords: Catalyst deactivation; Reaction heat effect; Resistance to carbon deposition; Resistance to particle sintering; Subsurface carbon

1. Introduction

Catalyst deactivation, namely the loss of catalytic activity and/or selectivity as a function of time on stream, is a challenge of great concern in industrial processes, which incur substantial costs due to process shutdown and catalyst replacement.[1,2] There are many intrinsic mechanisms for catalyst deactivation,[3,4,5] with the most widely encountered mechanisms being deposition of detrimental carbonaceous species and thermal sintering of metal particles.[6,7] Importantly, the external compensation temperature (i.e., the average reaction temperature) can be relatively low yet the phenomenon of coking and metal agglomeration can still be observed.[8,9,10] This could be associated with a natural nonlinear matching between reaction heat generation and heat transfer, in which the reaction heat changes in a nonlinear exponential form, while the heat transfer rate of the system is directly proportional to the heat transfer area and temperature gradient (so varies linearly) and is affected by multi-phase flow, radiation and other processes. The mismatching leads to the instantaneous accumulation of heat generated by an exothermic process and thus provides the energy for chemical bond breaking, carbon chain growth and metal atom migration. Consequently, in addition to the design of a reaction engineering system (such as condensate, reactor type, heat transfer area etc),[11,12,13] an ability to realize rapid heat transfer from the microscale (namely catalyst structure design) to avoid the occurrence of side reactions is also significant. Recently, Miao et al.[14] explored the influence of support structure on an exothermic reaction, and found that the modification of an alumina array increased the number of active sites which in turn, effectively decreased the localized heat production rate, thereby avoiding the formation of hot spots in the catalyst. This study demonstrated that the regulation of catalyst microstructure could reduce the accumulation of reaction heat on active site.

In some catalytic process, a product of reaction (a) can be a reactant in reaction (b), and the presence of reaction (b) makes reaction (a) possible, which can be called a

coupled process. Coupled reactions generally involve an endothermic reaction which is stimulated by heat released from an exothermic reaction and such processes have attracted extensive attention.[15, 16, 17] For instance, Chen et al.[18] coupled CO_2 and N_2 in H_2O to generate urea, which occurred via the production of C–N bonds through reaction between adsorbed and activated N_2 and CO. Inspired by the above research idea (i.e., utilizing heat from an exothermic reaction to supply energy for a beneficial endothermic process), we have considered how this might be used to develop improved selective hydrogenation catalysts. In this case, the exothermic reaction is hydrogenation of acetylene and the endothermic reaction is dissociation of acetylene which can lead to the structural modification of active metal particles (i.e., carbide formation).

In this work, two analogous samples with different Pd particle size were explored for the strong exothermic selective hydrogenation of acetylene. By combining systematic reaction studies with materials characterization, the essential relationship between metal dispersion and localized reaction heat was understood. Moreover, by utilizing the reaction heat, exothermic and endothermic reaction were coupled, resulting in the evolution of a novel supported Pd catalyst, which could further improve catalytic activity, selectivity and stability by inhibiting both particle agglomeration and deposition of detrimental carbonaceous species.

2. Experimental

2.1 Catalyst preparation. 1 wt. % Pd nanoparticles supported on carbon nanofiber (PR24-HHT, Applied Sciences Inc.; CNF) were synthesized by conventional impregnation as reported previously.[19] The precursor was reduced at either 250 or 550 ^oC in 10% H_2/N_2 for 1h to obtain two materials denoted as Pd/CNF-H-250 and Pd/CNF-H-550. As described later these materials possessed different Pd particle sizes. These reduced Pd samples were then treated in the temperature range of 50-250^oC (25^oC increments, 5h time on stream at each temperature) in a flow of 0.6%C_2H_2/5.4% C_2H_4/1.2%H_2/balance N_2 with a space velocity of 240000 h^{-1}. Following the entire sequence these samples were denoted as T-Pd/CNF-H-250 and T-Pd/CNF-H-550.

2.2 Catalytic testing. 0.02 g of catalyst diluted with quartz sand was tested in a fixed-bed microreactor at 1 bar in a gas stream of 0.6% C_2H_2/5.4% C_2H_4/1.2% H_2/balance N_2 with gas hourly space velocity (GHSV) of 60000-240000 h^{-1}. 5h time on stream was permitted for tests at each temperature in 50-250°C temperature range (25°C increments). Propane was employed as an internal standard. The analysis of products was performed online using a gas chromatograph (Perkin-Elmer Clarus 580) equipped with an elite alumina capillary column and a Flame Ionization Detector (FID). At least three tests for each point were carried out to obtain the quantitative measure of raw conversion/selectivity data repeatability. Equations for calculating acetylene conversion, ethylene and ethane selectivity were given as following:

$$Acetylene\ conversion = \frac{Acetylene\ (inlet) - Acetylene\ (outlet)}{Acetylene\ (inlet)} \quad \text{(Formula 1)}$$

$$Ethylene\ selectivity = \frac{Ethylene\ (outlet) - Ethylene\ (inlet)}{Acetylene\ (inlet) - Acetylene\ (outlet)} \quad \text{(Formula 2)}$$

$$Ethane\ selectivity = \frac{Ethane\ (outlet) - Ethane\ (inlet)}{Acetylene\ (inlet) - Acetylene\ (outlet)} \quad \text{(Formula 3)}$$

The selectivity to oligomers was calculated based on carbon balance.

2.3 Characterization. The morphology, size and structure of the samples were assessed using a JEOL 2100F microscope operating at 200 kV in transmission mode (TEM). Elemental analysis for Pd was carried out using a Shimadzu ICPS-7500 Inductively Coupled Plasma Atomic Emission Spectrometer (ICP-AES). Thermogravimetric analysis (TG) was utilized to measure the carbon species on the surface of catalysts. TGA was performed using a TG/DTA X70 thermogravimetric analyzer (NETZSCH) that can heat samples in the range of 25-600°C in flowing air. CO chemisorption was conducted on a Micrometrics ChemiSorb 2920 instrument equipped with 50 μL loop. CO/Pd average stoichiometry of 1 was used for the calculation of dispersion.[20] X-ray Photoelectron Spectroscopy (XPS) was carried out using a Thermo VG ESCALAB 250 spectrometer equipped with Al Kα anode to obtain insight into electronic structure with C 1s peak at 284.6 eV as a calibration. XRD patterns were collected using a Shimadzu XRD-6000 instrument with Cu-Kα radiation (λ = 1.5418 Å). Raman analysis was performed by using a HORIBA Jobin Yvon HR800

Raman spectrometer to analyze the nature of carbon support, in which 532 nm argon ion laser was employed as the excitation source.

3. Result and discussion

3.1 Catalyst structure

Two distinct Pd/CNF catalysts were obtained by impregnating and reducing at 250 and 550ºC. The formation of Pd nanoparticles after reduction at 550ºC is confirmed by XRD (Figure S1) with good agreement between the observed 2θ values and those expected (PDF#46-1043, 2θ=40.1º for (111) facet in Pd). Representative high resolution TEM images of Pd/CNF-H-550 catalyst and the corresponding size distributions obtained by counting more than 200 particles from TEM micrographs are presented in Figure 1A. The majority of particles (ca. 190) are observed to be 1-6 nm in size, although a small number of larger particles (>7 nm; more than 30) appears. The particle size distribution determined from TEM gives a mean particle diameter of 3.7 nm (Table S1). Whilst this type of average is generally used in catalysis, the volume-weighted average particle size (8.5 nm) can also be considered since it gives greater weighting to smaller number of large particles. When using this approach, the particle size correlates well with the crystallite size estimated from XRD by application of Scherrer equation (8.0 nm). Pd nanoparticles reduced at 250ºC has previously been characterized in detail with results reported elsewhere.[21] It is important to appreciate that Pd precursor is also transformed into the active phase upon reduction at 250ºC but possessing smaller Pd particles with a mean particle diameter of 1.6 nm (Figure 1B and Table S1). Figure S2 shows Raman spectra, in which two main bands with a shoulder are observed at 1350, 1580 and 1615 cm^{-1}. These former two are attributable to D band indicating lattice disorder and G band responsible for E_{2g} mode of graphite, while the latter is related to D′ band, being the characteristic for relatively low disorder structures. As expected, the intensity ratio of I_D/I_G in Pd/CNF-H reduced at 550ºC is basically consistent with that of Pd/CNF-H-250, indicating that the nature of carbon support is not affected under different reduction condition.

3.2 Selective hydrogenation of acetylene

Catalytic evaluation was firstly conducted over Pd/CNF-H-550 sample as a function of reaction temperature (50-250^{o}C) at a fixed pressure (1 bar) and gas hourly space velocity of 60000 h^{-1}. To demonstrate that the essentially same raw conversion and selectivity are obtained, namely the data repeatability,[22] the error bars are given from three parallel experiments. Note that the reaction begins with a period at 50^{o}C, prior to the reaction temperature increasing sequentially in 25^{o}C increments up to 250^{o}C. At the initial reaction temperature of 50^{o}C, acetylene conversion is incomplete and limited to 50% (see Figure 2A). This level of conversion leads to ethylene and ethane being produced in approximately equal proportions with relatively little oligomer formation (*ca.* 5%). At higher temperature (i.e., 75^{o}C) complete acetylene conversion is observed, while the product distribution noticeably shifts towards ethane and oligomers with ethylene selectivity becoming negative (i.e., a portion of the ethylene in the feed gas is also converted). When the reaction temperature reaches or exceeds 175^{o}C, the selectivity shifts towards ethylene with a corresponding decrease in ethane selectivity. Such an observation may be indicative of thermodynamic selectivity since the strength of alkyne adsorption is larger than the alkene (i.e., as temperature increases it becomes harder for ethylene to adsorb and react). However unfortunately, the production of oligomers remains at a high level and thus leads to the decrease of activity at 250^{o}C.

In order to decrease the production of oligomers/green oil, further tests were performed but with higher space velocity/decreased contact time. GHSV was varied from 60,000 to 240,000 h^{-1} by changing the linear gas flow rates and results are presented in Figure 2B and 2C. At 50^{o}C, the space velocity has an impact on the initial activity with a decrease in acetylene conversion at higher GHSV. With increasing temperature, the catalyst shows a similar trend with that at a GHSV of 60,000 h^{-1}. Increasing the space velocity to ca. 240000 h^{-1} has a positive effect on ethylene selectivity (although the value is still negative). However, increasing space velocity does not significantly reduce the quantity of oligomers formed and as a result the decrease of activity is still observed at end of the reaction sequence at 250^{o}C. The above results indicate that when the catalyst structure is fixed, the impact of the

microenvironment change of the operating catalyst (i.e., GHSV) is limited.

Furthermore, the catalytic behavior over the catalyst with smaller particle size was also evaluated by varying the space velocity from 60000 to 240000 h^{-1} (Figure 3). Complete acetylene conversion was observed for this sample even at 50°C and this is likely related to the samples with higher dispersion/greater number of active sites (compare Figure 2 & 3). More importantly, relative to Pd/CNF-H-550 catalyst, Pd/CNF-H-250 sample exhibits the positive selectivity of ethylene, which indicates that Pd/CNF-H-250 sample is inherently more selective than that reduced at 550°C. Note that this sample at a space velocity of 240000 h^{-1} has been reported in the previous work.[21] In order to prove the repeatability of the data and facilitate readers to compare the performance under different GHSV, this sample was re-performed at 240000 h^{-1} GHSV and 250°C. Ethylene selectivity obtained at the above reaction condition in Figure 3C is ca. 74.0%, which is basically coincident with previous results, proving the accuracy of the data again. Also, it is found that Pd/CNF-H-250 significantly reduces the formation of oligomers when operating at GHSV of 240000 h^{-1}. When comparing the two samples at equivalent space velocity, the sample with smaller Pd particles appears to form less oligomers. These results indicate that Pd/CNF-H-250 and Pd/CNF-H-550 samples perform distinctly differently despite having what might otherwise be considered a relatively small dissimilarity in particle size (1.6 vs 3.7 nm). The key is to therefore understand the origin of this difference.

3.3 Effect of in situ pretreatment on catalyst structure and performance

To begin with, the particle size before and after the first reaction (namely in situ pretreatment) was characterized. It is found that for Pd/CNF-H-550, the particle size increases notably after reaction (4.6 nm after vs 3.7 nm before), while Pd/CNF-H-250 sample exhibits no significant change (1.8 nm after vs 1.6 nm before) based on HRTEM results (Figure 4). When this information is combined with the catalytic results it would suggest that the control of metal dispersion can limit carbon accumulation whilst also hindering metal sintering caused by a thermal effect.[23]

To verify how dispersion influences a catalysts ability to handle heat released during

a reaction, we calculate the exothermic rate for the acetylene hydrogenation at different temperatures as below:[24]

$$Q_R = C_{C_2H_2} \times A \times \Delta H \quad \text{(Formula 4)}$$

$$Q_{site} = \frac{C_{C_2H_2} A}{m \times w \times D} \Delta H \quad \text{(Formula 5)}$$

where Q_R represents the exothermic rate of the catalyst, $C_{C_2H_2}$ stands for conversion, A is the C_2H_2 flow rate, ΔH is the enthalpy change for acetylene hydrogenation, Q_{site} represents the exothermic rate per active site, m is catalyst mass, w stands for metal loading and D is metal dispersion (calculated from pulse chemisorption, Table S1). As presented in Figure 5A, the Q_R value is larger for Pd/CNF-H-250 (0.186 kJ s^{-1}) than for Pd/CNF-H-550 (0.167 kJ s^{-1}). However, interestingly and importantly, the Q_{site} values for Pd/CNF-H-250 is lower than that for Pd/CNF-H-550. Especially, for Pd/CNF-H-550 catalysts with large particles, a part of ethylene is also hydrogenated to generate the ethane (Figure 2). That is to say, the ethylene hydrogenation as the exothermic reaction could also lead to the heat effect. But unexpected, Q_{site}' as the exothermic rate from ethylene hydrogenation on per active site, is difficult to be accurately calculated based on the calculation formula. This is since not only ethylene in the feed gas could be hydrogenated, but also the ethylene produced from acetylene hydrogenation also undergoes reaction to ethane, which influences the conversion and flow rate of ethylene on the catalyst surface (the ethylene inlet is not equivalent to converted ethylene). However, as long as ethylene hydrogenation occurs no matter how much heat is generated, the actual exothermic rate per single active site for Pd/CNF-H-550 should be higher than the exhibited one at present in Figure 5B (It is not sure a linear superposition, but the released heat from the hydrogenation of acetylene and ethylene must be higher than the individual one). That is to say, the actual exothermic rate per single active site for Pd/CNF-H-250 should be much lower than that for Pd/CNF-H-550. This could be associated with higher metal dispersion which increases the number of reaction sites and in turn effectively reduces the heat produced per active site. If less heat is produced per active site then this limits accumulation of reaction heat and consequently reduces the generation of hot spots which could otherwise promote

sintering and polymerization to form detrimental carbonaceous species.[25] Based on the expected sintering mechanism, when heat is effectively dissipated, the localized metal particle temperature won't reach Tammann temperature (~0.5 T_m) [1] and hence Ostwald ripening won't occur[26] thereby leading to greater sintering resistance.

According to carbon deposition mechanisms,[27,28] in addition to harmful carbon species (graphitic carbon), some harmless or beneficial carbon species (carbide or a carbon overlayer) can be produced in a reaction process at lower temperature. In detail, carbon species can enter into the octahedral lattice of Pd crystallites to form subsurface carbon, which suppresses the formation of subsurface hydrogen associated with alkyne over-hydrogenation. Furthermore, when the amount of carbon species increases to a certain extent, a thin but permeable carbon overlayer will be generated, which allows the diffusion of reactants to reach active sites yet can influence the adsorption modes of reactant molecules, potentially improving selectivity. It should be noted that typically the subsurface carbon atoms are formed from decomposition of C2 species in the feed for acetylene hydrogenation. [29] On the basis of thermodynamic data and thermodynamic principles, this is an endothermic process (Formula 6), requiring a certain amount of heat to break the C-C bond.

$$\Delta H = \Sigma E_{(reactant)} - \Sigma E_{(product)} \qquad \text{(Formula 6)}$$

where E represents the bond energy and Σ stands for the sum of all bond energies. However, if too much heat is provided then polymerization of acetylene can take place via splitting of an ethylene carbon–carbon bond leading to green oil or surface carbene species, respectively. Moreover, the latter could be further hydrogenated to generate methane or dehydrogenated and polymerized to form a harmful type of carbon species. As the amount of carbon deposition by this route increases (i.e., thicker deposits of green oil or deposited carbon species), the accessibility of acetylene to active sites decreases; that is to say that fewer reactant molecules may access suitable sites to react with hydrogen, thus leading to the observed deactivation.[30]

Based on this and by assuming that little or no instantaneous heat accumulates on the highly dispersed catalyst, the reaction feed involving $C_2H_2/C_2H_4/H_2$ is passed into the

reactor for temperature programmed treatment. The obtained catalyst (denoted as T-Pd/CNF-H-250) was characterized by XRD analysis to explore the crystal structure (see Figure 6A). Interestingly, it is found that Pd (111) peak position shifts towards a lower angle to 38.7° with regard to the freshly reduced sample (40.1°, see Figure S1), suggesting the formation of a PdC_x phase during the temperature programmed treatment with C atoms able to enter into the subsurface of Pd particles[31] (theoretically proven to be energetically favorable[32]). Furthermore, Pd/CNF-H-550 was also treated using the same temperature programmed process. The obtained catalyst still displays the characteristic of Pd metal at 2θ of 40.1° (Figure 6A) but with very weak intensity and with no evidence to suggest that a carbide phase can form. Instead, it could be noted that Pd nanoparticles in this sample are instead covered by deposited oligomers, which lead to the blockage of active Pd sites and thus trigger more rapid deactivation.[33] It should be noted that the deposited carbonaceous species cannot be effectively observed by XRD due to the overlap with the diffraction of C substrate, although they may also be amorphous in nature.[34] Moreover, the surface and near-surface information of samples were further investigated by using X-ray photoelectron spectroscopy (XPS). After in situ temperature programmed treatment, carbon atom enters the subsurface of Pd particles to form Pd carbide at 283.6 eV,[35] which has been confirmed in previous report.[21] However, the treatment for bigger Pd particles in T-Pd/CNF-H-550 leads to a rather broad peak observed around 284.6 eV with increasing peak intensity relative to Pd/CNF-H-550, shown in the C1s spectral region in Figure 6B. Also, the peak shape and position are identical to the type of carbon in graphene, indicating the large amount of coke forms except for the features of CNF support.[36]

TG measurement of the reduced Pd/CNF-H before and after in situ pretreatment was also performed. Since TG data for T-Pd/CNF-H-250 had been reported in the previous work,[21] the corresponding results is only briefly summarized here to facilitate the reader to understand. For the fresh Pd catalyst, no any weight loss is observed. However, in terms of T-Pd/CNF-H-550 catalyst, massive weight loss is observed at 350^{o}C (Figure S3), indicating that the harmful carbon species deposits on larger Pd catalyst, which is well agreement with XPS results. However differently, T-

Pd/CNF-H-250 catalyst previous reported exhibited a smaller amount of weight loss at lower temperature of ca. 250ºC, which was attributed to the combustion of harmless carbon, such as carbon atoms penetrating into the subsurface of Pd nanoparticles (combined with XPS analysis). The above data indicate that more effective heat dissipation results in multiple effects. Thermal sintering is lessened, while the nature of carbon deposition is also changed, both of which are beneficial effect on catalytic performance.

The novel catalyst structure obtained by temperature programmed reaction treatment was explored for the selective hydrogenation of acetylene at 240000 h^{-1} GHSV in the 50-250ºC range studied for 5h time on stream at each temperature. Reaction with acetylene over T-Pd/CNF-H-250 (Figure 7A) exhibits full conversion at all temperatures. Note that the space velocity used is high for acetylene hydrogenation hinting that H-Pd/CNF-H-250 maintains high activity. Interestingly, ethylene selectivity is significantly higher than observed prior to the treatment (compare Figure 7A with Figure 3C). For example, at 250ºC, ethylene is generated with 93.2% selectivity with only a little ethane as side products (6.0%). Furthermore, oligomer selectivity is observed to be exceptionally low at this temperature (*ca.* 0.8%). This trend of performance change is basically in agreement with the previous report.[21] The novel T-Pd/CNF-H-250 catalyst not only reduces the generation of oligomers, but also further promotes the selectivity of ethylene, attributed to the formation of the aforementioned carbide phase. The long period testing over 50h was assessed at relatively low conversion.[37] T-Pd/CNF-H-250 catalyst gives the satisfactory stability, in which ca. 76% conversion and ca. 85% selectivity are maintained for 50h. An understanding of why this particular catalyst exhibits exceptional performance is not trivial. Firstly, the highly dispersed active metal limits the amount of localized reaction heat that can build up such that controlled acetylene decomposition leads to the formation of C atoms and subsequent subsurface C species. The presence of this species modifies the d-band center of Pd such that it apparently favors the ethylene desorption, which has been confirmed by XPS and DFT calculation.[21]

TG analysis was performed over spent T-Pd/CNF-H-250 catalysts in an air atmosphere. As shown in Figure 7C, relative to fresh T-Pd/CNF-H-250 sample reported in previous work (ca. 11% of weight loss)[21], there is no significant increase in the amount of combustible carbonaceous deposits after 50 h time on stream. This would be consistent with the exceptionally low oligomer selectivity observed for this sample at 250 °C (Figure 7A) and at least partially explains the strong stability data (Figure 7B). For completeness it is also important to assess the performance of T-Pd/CNF-H-550 sample. This material shows lower activity (Figure 7D) and evidence of deactivation at higher temperature, which is attributed to particle sintering and greater oligomer as the precursor for polymeric carbon species, confirmed by HRTEM, XPS and TG results (Figure S4-S6). This carbon species build up on active sites resulting in deactivation over a relatively short time of stream.

In summary, Pd catalysts with different size were fabricated and applied in the highly exothermic selective hydrogenation of acetylene. It was found that with larger Pd particles (mean size 3.7 nm), large amounts of oligomers formed and Pd particles agglomerated during catalytic testing. These effects were not mitigated by operating at higher space velocity and thus resulted in deactivation by a combination of mechanisms (Scheme 1). Interestingly, when Pd particle size decreased (mean size 1.6 nm), little or no sintering was observed. Smaller Pd particles yielded smaller amounts of oligomers/green oil at an equivalent space velocity. This could be ascribed to less localized heat built up since higher dispersion increased the number of active sites. Furthermore, we coupled the exothermic process (acetylene hydrogenation) and endothermic process (acetylene dissociation) by utilizing the reaction heat to construct novel supported Pd catalysts with subsurface carbon modification in a controlled manner. The presence of subsurface carbon on Pd further enhanced ethylene selectivity whilst also limiting oligomer selectivity and enhancing catalyst lifetime. This work therefore demonstrates two interrelated deactivation mechanisms (sintering and coking) can be influenced and to some extent controlled/utilized to create more effective catalytic materials. Higher dispersion inherently limits heat accumulation which makes it more feasible to retain carbon in a beneficial manner for Pd catalysts in acetylene

hydrogenation. It is thought that this level of insight will be useful for the development of catalysts for other reactions as well.

ASSOCIATED CONTENT

Supporting Information

XRD patterns, particle sizes, dispersion and Raman spectra of Pd/CNF catalysts; HRTEM images, XPS spectra and TG profiles of T-Pd/CNF-H-550 after reaction.

Author Contributions

Y. Liu conceived and designed the experiment. S. Weng and A. McCue synthesized the experimental samples and carried out most of the characterization, as well as the catalytic reactions. H. Yu and B. Fu conducted part of experiments and structural analysis. Y. Liu, A. McCue, Y. He and J. Feng discussed the results and wrote the manuscript. D. Li and X. Duan provided the ideas and funding support.

Notes

The authors declare no competing financial interest.

ACKNOWLEDGMENT

This work was financially supported by National Key R&D Program of China (2021YFB3801600), National Natural Science Foundation of China (21908002), and Fundamental Research Funds for the Central Universities (buctrc201921, JD2223).

Figures

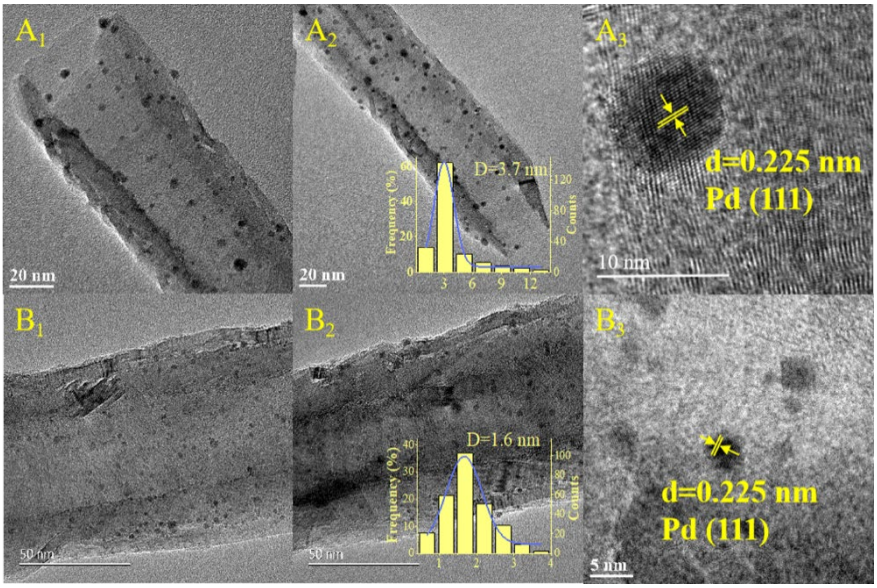

Figure 1 HRTEM images of (A) Pd/CNF-H-550 and (B) Pd/CNF-H-250 with the size distribution inset by randomly selecting more than 200 particles in different regions

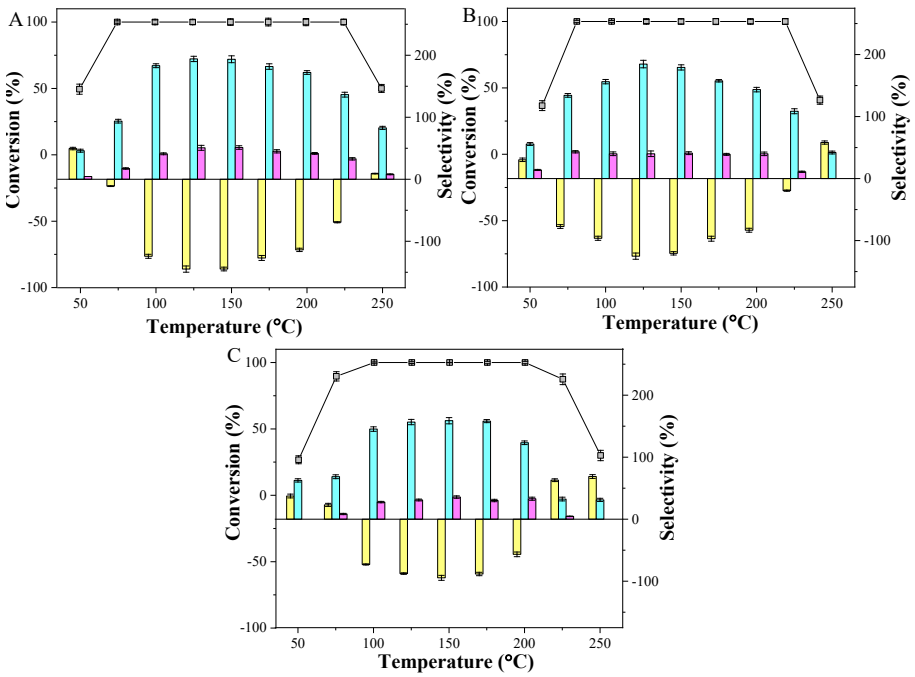

Figure 2 Conversion (gray), selectivity of ethylene (yellow), ethane (cyan), and oligomers (pink) versus temperature over Pd/CNF-H-550 at GHSV of (A) 60000 h^{-1} (B) 120000 h^{-1} (C) 240000 h^{-1}

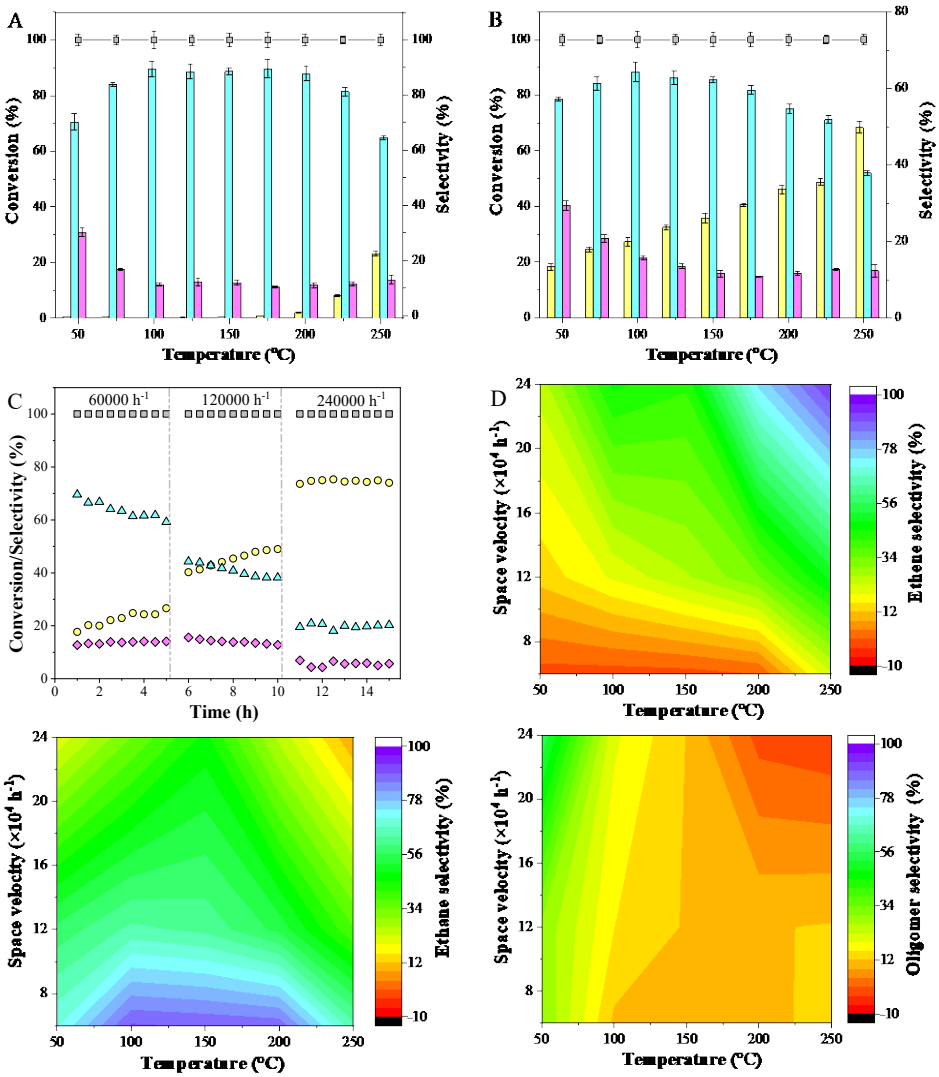

Figure 3 Conversion (gray), selectivity of ethylene (yellow), ethane (cyan), and oligomers (pink) versus temperature over Pd/CNF-H-250 at GHSV of (A) 60000 h^{-1} (B) 120000 h^{-1} (C) Catalytic performances at 250°C with increasing space velocity. Color contour maps summarizing selectivity of (D) ethylene (E) ethane (F) oligomers at different temperatures and space velocities

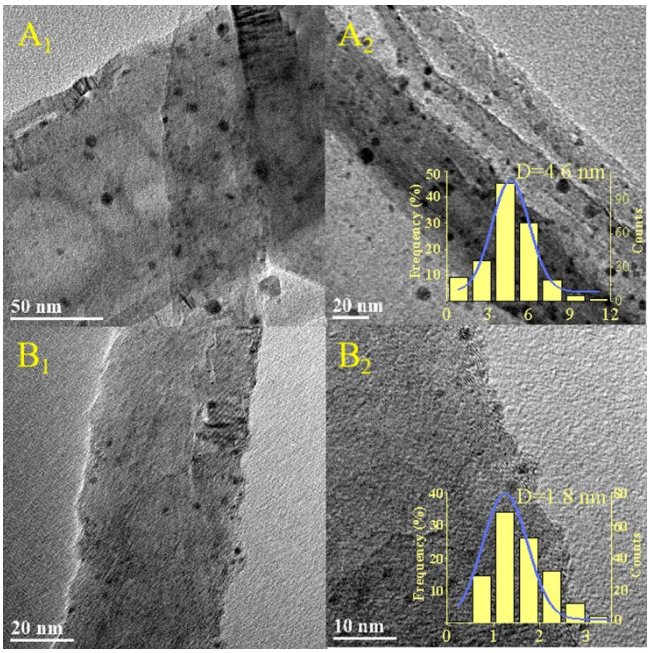

Figure 4 HRTEM images of (A) Pd/CNF-H-550 (B) Pd/CNF-H-250 after the first reaction (namely *in situ* pretreatment) with the size distribution inset by randomly selecting more than 200 particles in different regions

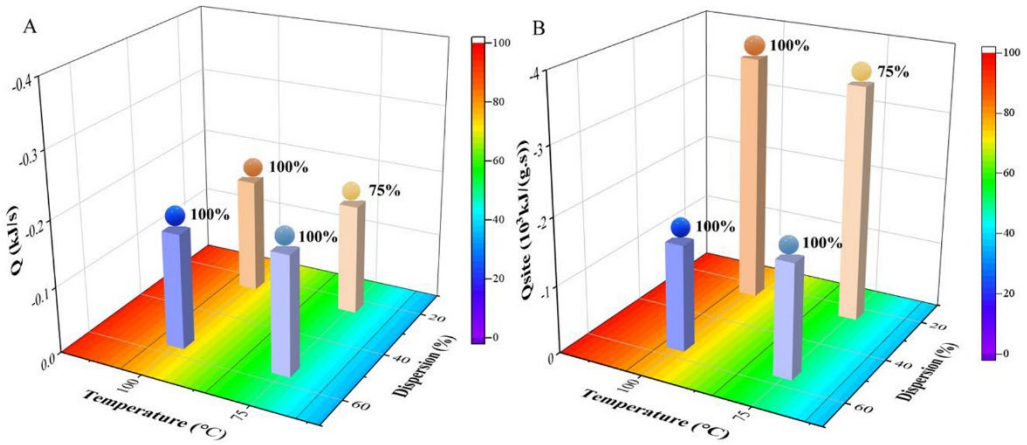

Figure 5 (A) Exothermic rate of acetylene hydrogenation (B) exothermic rate per single active site in acetylene hydrogenation under different reaction temperatures for Pd/CNF-H-250 (blue) and Pd/CNF-H-550 (orange). The values (100% and 75%) on the column represent the conversion at the corresponding temperature

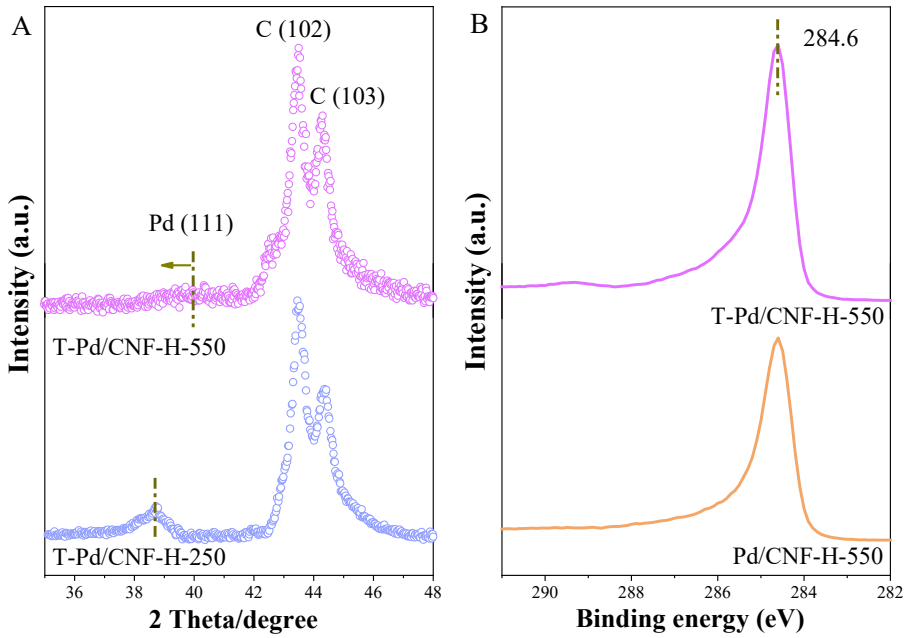

Figure 6 (A) XRD patterns of T-Pd/CNF-H-250 and T-Pd/CNF-H-550 samples (B) XPS spectra of C 1s over Pd/CNF-H-550 before and after in situ pretreatment

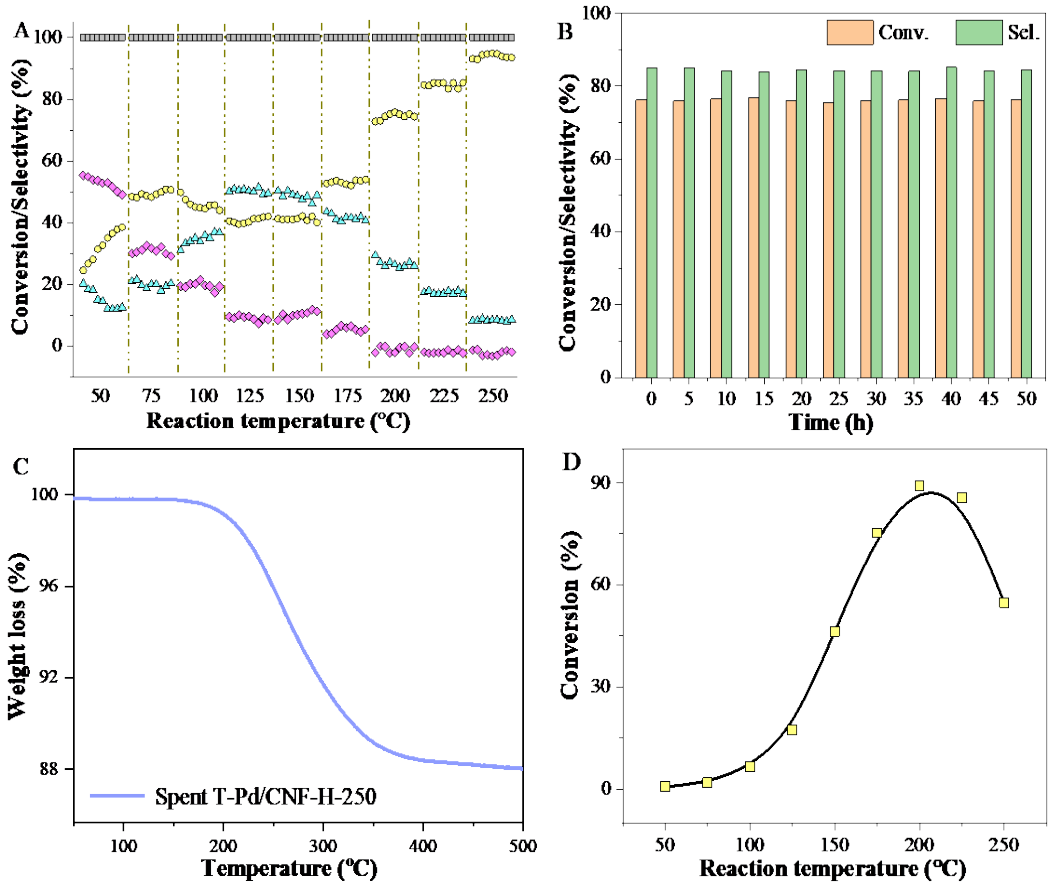

Figure 7 (A) Acetylene conversion (grey squares), selectivity of ethylene (yellow circle), ethane (cyan triangle), and oligomers (pink diamond) as a function of temperature (B) stability over T-Pd/CNF-H-250 sample at 240000 h^{-1} GHSV (C) TG profile of spent T-Pd/CNF-H-250 catalysts (D) Acetylene conversion versus temperature over T-Pd/CNF-H-550

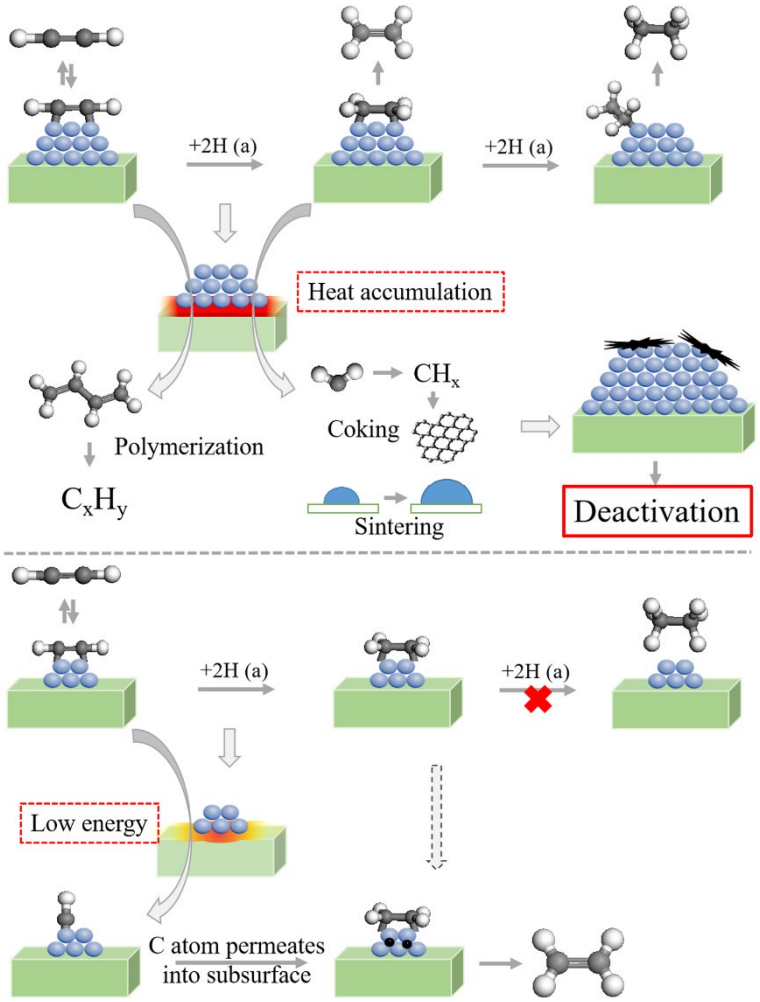

Scheme 1 Top - Proposed deactivation mechanism of Pd/CNF catalyst with larger metal particles. Bottom – Proposed mechanism by which a highly stable and selective Pd/CNF catalyst can form when beginning with smaller metal particles

Graphical abstract

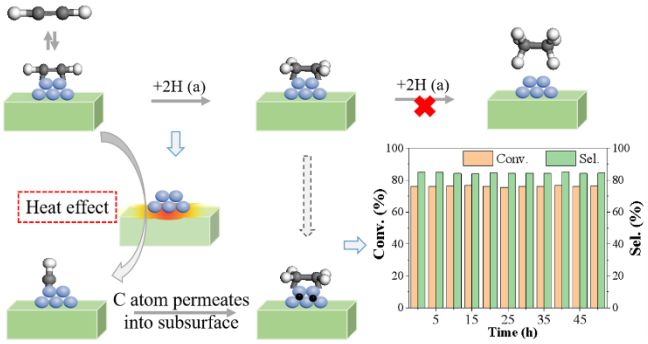

References

1 S. Hu, W. X. Li, Sabatier principle of metal-support interaction for design of ultrastable metal nanocatalysts, Science. 374 (2021) 1360-1365.

2 C. H. Bartholomew, Mechanisms of catalyst deactivation, Appl. Catal. A-Gen. 212 (2001) 17-60.

3 M. D. Argyle, C. H. Bartholomew, Heterogeneous catalyst deactivation and regeneration: a review. Catalysts. 5 (2015) 145-269.

4 J. A. Moulijn, A. E. van Diepen, F. Kapteijn, Catalyst deactivation: is it predictable? what to do? Appl. Catal. A-Gen. 212 (2001) 3-16.

5 R. Ouyang, J. X. Liu, W. X. Li, Atomistic theory of ostwald ripening and disintegration of supported metal particles under reaction conditions, J. Am. Chem. Soc. 135 (2013) 1760-1771.

6 E. E. Wolf, F. Alfani, Catalysts deactivation by coking, Catal. Rev. Sci. Eng. 24 (1982) 329-371.

7 Y. Dai, P. Lu, Z. Cao, C. T. Campbell, Y. Xia, The physical chemistry and materials science behind sinter-resistant catalysts, Chem. Soc. Rev. 47 (2018) 4314-4331.

8 A. J. McCue, J. A. Anderson, Recent advances in selective acetylene hydrogenation using palladium containing catalysts, Front. Chem. Sci. Eng. 9 (2015) 142-153.

9 Y. N. Liu, J. T. Feng, Y. F. He, J. H. Sun, D. Q. Li, Partial hydrogenation of acetylene over a NiTi-layered double hydroxide supported PdAg catalyst, Catal. Sci. Technol. 5 (2015) 1231-1240.

10 Y. N. Liu, Y. F. He, D. R. Zhou, J. T. Feng, D. Q. Li, Catalytic performance of Pd-promoted Cu hydrotalcite-derived catalysts in partial hydrogenation of acetylene: effect of Pd–Cu alloy formation, Catal. Sci. Technol. 6 (2016) 3027-3037.

11 T. J. Taha, B. L. Mojet, L. Lefferts, T. H. van der Meer, Effect of carbon nanofiber surface morphology on convective heat transfer from cylindrical surface: Synthesis, characterization and heat transfer measurement, Int. J. Therm. Sci. 105 (2016) 13-21.

12 T. Esaki, N. Kobayashi. Study on the cycle characteristics of chemical heat storage with different reactor module types for calcium chloride hydration, Appl. Therm. Eng. 171 (2020) 114988.

13 S. Adera, L. Naworski, A. Davitt, N. K. Mandsberg, A. Shneidman, J. Alvarenga, J. Aizenberg, Enhanced condensation heat transfer using porous silica inverse opal coatings on copper tubes, Sci. Rep. 11 (2021) 10675.

14 C. L. Miao, L. Y. Cai, Y. F. Wang, X. J. Xu, J. R. Yang, Y. F. He, D. Q. Li, J. T. Feng, Array modified molded alumina supported PdAg catalyst for selective acetylene hydrogenation: intrinsic kinetics enhancement and thermal effect optimization, Ind. Eng. Chem. Res. 60 (2021) 8362-8374.

15 Y. M. Bruschi, E. López, M. N. Pedernera, D. O. Borio, Coupling exothermic and endothermic reactions in an ethanol microreformer for H_2 production, Chem. Eng. J. 294 (2016) 97-104.

16 M. R. Rahimpour, M. R. Dehnavi, F. Allahgholipour, D. Iranshashi, S. M. Jokar, Assessment and comparison of different catalytic coupling exothermic and endothermic reactions: A review, Appl. Energy 99 (2012) 496-512.

17 F. Yin, S. Ji, H. Mei, Z. Zhou, C. Li, Coupling of highly exothermic and endothermic reactions in a metallic monolith catalyst reactor: A preliminary experimental study, Chem. Eng. J. 155 (2009) 285-291.

18 C. Chen, X. Zhu, X. Wen, Y. Zhou, L. Zhou, H. Li, L. Tao, Q. Li, S. Du, T. Liu, D. Yan, C. Xie, Y. Zou, Y. Wang, R. Chen, J. Huo, Y. Li, J. Cheng, H. Su, X. Zhao, W. Cheng, Q. Liu, H. Lin, J. Luo, J. Chen, M. Dong, K. Cheng, C. Li, S. Wang, Coupling N_2 and CO_2 in H_2O to synthesize urea under ambient conditions, Nat. Chem. 12 (2020) 717-724.

19 B. Bachiller-Baeza, A. Iglesias-Juez, E. Castillejos-López, A. Guerrero-Ruiz, M. Michiel, M. Fernandez-Garćía, I. Rodríguez-Ramos, Detecting the genesis of a high-performance carbon-supported Pd sulfide nanophase and its evolution in the hydrogenation of butadiene, ACS. Catal. 5 (2015) 5235-5241.

20 W. Huang, J. R. McCormick, R. F. Lobo, J. G. G. Chen, Selective hydrogenation of acetylene in the presence of ethylene on zeolite-supported bimetallic catalysts, J. Catal. 246 (2007) 40-51.

21 Y. N. Liu, F. Z. Fu, A. McCue, W. Jones, D. M. Rao, J. T. Feng, Y. F. He, D. Q. Li, Adsorbate-induced structural evolution of Pd catalyst for selective hydrogenation of acetylene, ACS. Catal. 10 (2020) 15048-15059.

22 S. L. Scott, T. B. Gunnoe, P. Fornasiero, C. M. Crudden. To Err is Human; To Reproduce Takes Time. ACS Catal. 12 (2022) 3644−3650.

23 B. Fu, A. J. McCue, Y. Liu, S. Weng, Y. Song, Y. He, J. Feng, D. Li, Highly selective and stable isolated non-noble metal atom catalysts for selective hydrogenation of acetylene. ACS Catal. 2022, 12, 607-615.

24 W. Ru, Y. N. Liu, B. A. Fu, F. Z. Fu, J. Ting. Feng, D. Q. Li, Control of local electronic structure of Pd single atom catalyst by adsorbate induction, Small. (2021) 2103852.

25 M. M. Chen, K. L. Yan, Y. Q. Cao, Y. R. Li, X. H. Ge, J. Zhang, X. Q. Gong, G. Qian, X. G. Zhou, X. Z. Duan, Thermodynamics insights into the selective hydrogenation of alkynes in C_2 and C_3 streams, Ind. Eng. Chem. Res. 60 (2021) 16969-16980.

26 R. Ouyang, J. Liu, W. Li, Atomistic Theory of Ostwald Ripening and Disintegration of Supported Metal Particles under Reaction Conditions, J. Am. Chem. Soc. 135 (2013) 1760-1771.

27 M. T. Ravanchi, S. Sahebdelfar, S. Komeili, Acetylene selective hydrogenation: a technical review on catalytic aspects, Rev. Chem. Eng. 34 (2018) 215-237.

28 F. Viñes, C. Loschen, F. Illas, K. M. Neyman, Edge sites as a gate for subsurface carbon in palladium nanoparticles, J. Catal. 266 (2009) 59-63.

29 B. Yang, R. Burch, C. Hardacre, P. Hu, P. Hughes, Selective Hydrogenation of Acetylene over Pd−Boron Catalysts: A Density Functional Theory Study, J. Phys. Chem. C 118 (2014) 3664-3671.

30 M. T. Ravanchi, S. Sahebdelfar, M. R. Fard, S. Fadaeerayeni, P. Bigdeli, Pd-Ag/α-Al_2O_3 catalyst deactivation in acetylene selective hydrogenation process, Chem. Eng. Technol. 39 (2016) 301-310.

31 M. Crespo-Quesada, S. Yoon, M. S. Jin, A. Prestianni, R. Cortese, F. Cárdenas-Lizana, D. Duca, A. Weidenkaff, L. Kiwi-Minsker, Shape-dependence of Pd nanocrystal carburization during acetylene hydrogenation, J. Phys. Chem. C. 119 (2015) 1101-1107.

32 D. Teschner, Z. Révay, J. Borsodi, M. Hävecker, A. Knop-Gericke, R. Schlögl, D. Milroy, S. D. Jackson, D. Torres, P. Sautet, Understanding palladium hydrogenation catalysts: when the nature of the reactive molecule controls the nature of the catalyst active phase, Angew. Chem. Int. Ed. 120 (2008) 9414-9418.

33 M. Greluka, M. Rotkoa, S. Turczyniak-Surdackab, Comparison of catalytic performance and coking resistant behaviors of cobalt- and nickel based catalyst with different Co/Ce and Ni/Ce molar ratio under SRE conditions, Appl. Catal. A-Gen. 590 (2020) 117334.

34 K. H. Wu, D. W. Wang, I. R. Gentle, Revisiting oxygen reduction reaction on oxidized and unzipped carbon nanotubes, Carbon. 81 (2015) 295-304.

35 D. Teschner, E.Vass, M. Hävecker, et al, Alkyne hydrogenation over Pd catalysts: a new paradigm, J. Catal. 242 (2006) 26−37.

36 C. J. Weststrate, et al, Atomic and polymeric carbon on Co (0001): surface reconstruction, graphene formation, and catalyst poisoning, J. Phys. Chem. C. 116 (2012) 11575-11583.

37 S. L. Scott. A Matter of Life (time) and Death. ACS Catal. 8 (2018) 8597–8599.

Mitigating catalyst deactivation in selective hydrogenation by enhancing dispersion and utilizing reaction heat effect

Yanan Liu[1,2], Shaoxia Weng[1], Alan J. McCue[3], Baoai Fu[1], He Yu[1], Yufei He[1,2], Junting Feng[1,2], Dianqing Li[1,2,*] and Xue Duan[1]

[1]*State Key Laboratory of Chemical Resource Engineering, Beijing University of Chemical Technology, Beijing, 100029, China*

[2]*Beijing Engineering Center for Hierarchical Catalysts, Beijing University of Chemical Technology, Beijing, 100029, China*

[3]*Department of Chemistry, University of Aberdeen, Aberdeen AB24 3UE, U.K.*

* Corresponding authors

Address: *Box 98, 15 Bei San Huan East Road, Beijing, China, 100029*

Tel/Fax: +86 (10) 64436992;

E-mail address: lidq@mail.buct.edu.cn *(Dianqing Li)*

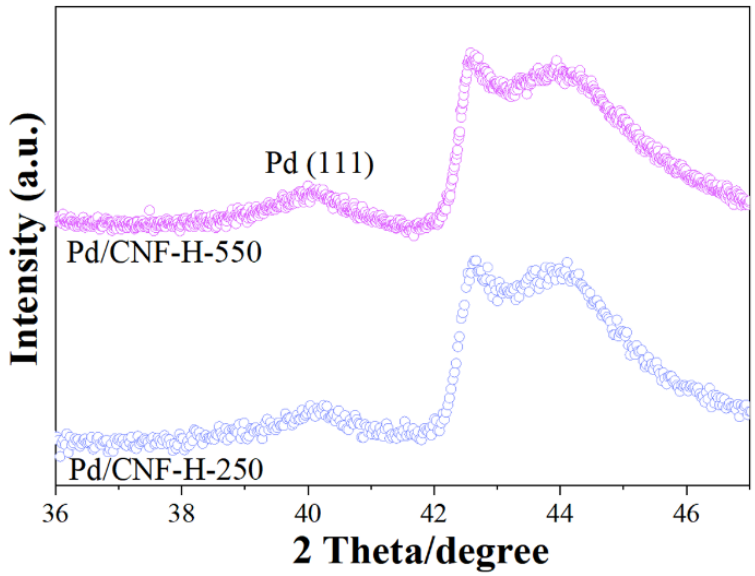

Figure S1 XRD patterns of Pd/CNF-H-550 and Pd/CNF-H-250

Table S1 Particle size and dispersion of Pd/CNF-H-550 and Pd/CNF-H-250

Catalysts	Particle size (nm) [a]	Dispersion (%)[b]
Pd/CNF-H-550	3.7	23.9
Pd/CNF-H-250	1.6	55.7

[a] Determined by HRTEM analysis; [b] Determined by CO chemisorption

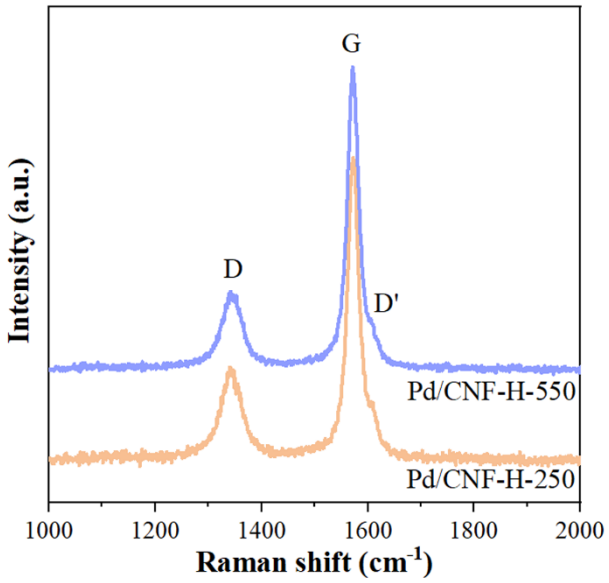

Figure S2 Raman spectra using an excitation energy of 532 nm for Pd catalysts reduced at different temperature

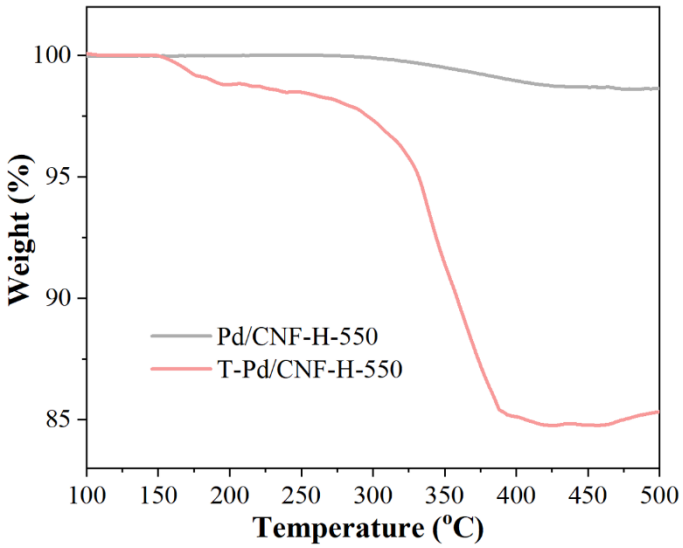

Figure S3 TG profiles of Pd/CNF-H-550 before and after the treatment

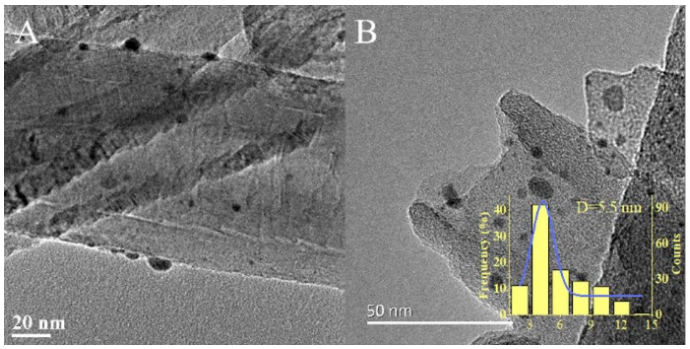

Figure S4 HRTEM images of T-Pd/CNF-H-550 after reaction

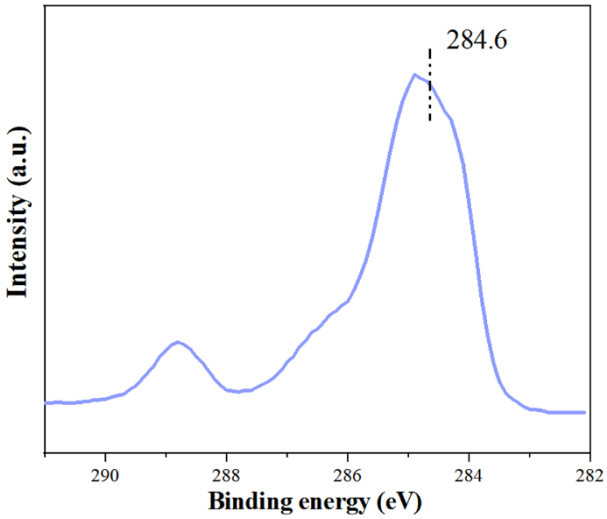

Figure S5 C 1s XPS spectra of T-Pd/CNF-H-550 after reaction

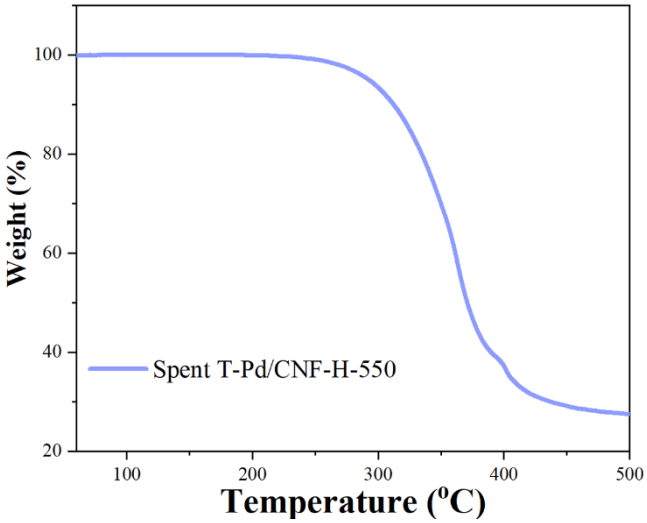

Figure S6 TG profiles of T-Pd/CNF-H-550 after reaction